Electrochromic Diffraction from Nanopatterned Poly(3-hexylthiophene)

Yuna Kim, Yoonjung Kim, Sehwan Kim, and Eunkyoung Kim*

Department of Chemical and Biomolecular Engineering, Yonsei University, 262 Seongsanno, Seodaemun-gu, Seoul 120-749, Korea

ARTICLE

ABSTRACT Poly(3-hexylthiophene) (P3HT) films were patterned by a soft lithography technique using a nanopatterned polydimethylsiloxane (PDMS) mold to generate one-dimensional (1D) grating and two-dimensional (2D) crossed line pillar patterns. The redox currents (i_p) were significantly increased due to the facilitated diffusion of ClO_4^- counterions associated with redox processes at the P3HT electrode as analyzing cyclic voltammetry (CV) was performed at different scan rates (ν). It was found that the diffusion coefficient (D_f, $cm^2\ s^{-1}$) for ion diffusion in the patterned electrode was much larger than that of the pristine P3HT electrode. Furthermore, the value of D_f in the 2D electrode was three times higher than that in a pristine film. As a result of such facilitated charge transport, the electrochromic (EC) properties of the patterned P3HT electrode were greatly enhanced and dependent on the dimension of the pattern. Thus, the electrochromic efficiency (E_e), including the coloration (E_c) and bleaching efficiencies (E_b), was higher as the dimension of the pattern was increased; E_e was maximized in the 2D patterned P3HT film. In a patterned cell, electrochromic diffraction was reversibly observed with a switching efficiency (R_{DE}) of 2 and 2.5 for the 1D and 2D patterned cells, respectively.

KEYWORDS: patterning · poly(3-hexylthiophene) · electrochromic · nanoimprint · PDMS

Electronic devices based on conducting polymers (CP) have attracted considerable attention because conjugated polymers can be easily processed with inexpensive technologies at low temperatures. The potential applications of CPs for organic electronic devices include solar cells, light-emitting diodes (LEDs), electrochromic (EC) devices, photodiodes, transistors, and biosensors.[1−5] The development of a faster and more integrated electrical or optical response has become a high priority. As such, the modification of an electroactive surface by nanostructures has been researched for switching or sensing devices.[6−8]

In electrochromic devices (ECDs), electrons are injected or extracted under an applied electric field while charge balancing counterions are simultaneously transported into or out of the EC layer.[9,10] The transport of electrons and ions is directly related to EC properties such as coloration efficiency and response time.[9−11] Recently, fast response times and high color contrast have reportedly been achieved with EC devices fabricated with a nanostructured EC electrode since the nanostructures can provide a large surface area. The increased surface area facilitates ion transport and provides more accessible reacting sites for the charge/discharge process.[8,10,12] Such a nanostructured EC electrode can be prepared through layer-by-layer (LBL) deposition[11,13] or by adopting nanotemplates such as anodized aluminum oxide (AAO),[14] TiO_2 nanoparticles,[8] Si nanowires,[10] and block copolymer templates.[15] As the charge transport in an EC device occurs vertically between the working and counter electrode, the design of a vertical EC nanostructure is indeed a challenge.

Various methods of fabricating conducting polymer nanostructures have been reported. Of the methods used, soft lithography using solution-processable conducting polymers can efficiently produce nanostructures with a large area.[16−19] However, its application to ECDs is rare.[18,19] In a report on the effect of nanoimprinting on the electrochromic properties of PEDOT:PSS,[18] improvements in both the response time and coloration efficiency were attained. However, to the best of our knowledge, there are no published reports on the direct effect of patterning in terms of charge transport through the patterned structures.

In this study, an EC device based on a nanopatterned EC electrode was fabricated. The EC electrode was prepared by directly nanoimprinting a pristine poly(3-hexylthiophene) (P3HT) film with a nanopattern replicated polydimethylsiloxane (PDMS) mold. Films with line gratings (1D) and pillars (2D) were examined to explore the charge transport and optical

*Address correspondence to eunkim@yonsei.kr.

Received for review July 14, 2010 and accepted August 16, 2010.

Published online August 23, 2010.
10.1021/nn1016378

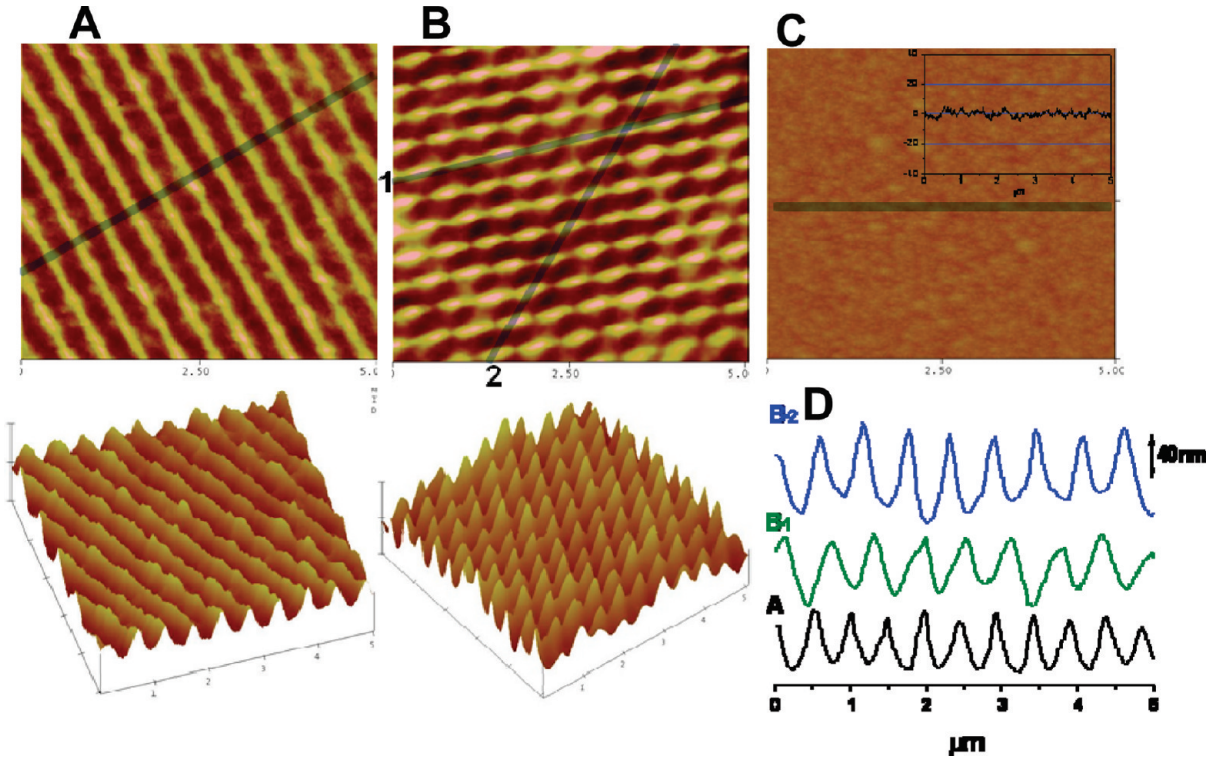

Figure 1. Atomic force microscope (AFM) images of single patterned P3HT film fabricated by imprinting at room temperature (A) and double patterned P3HT film (B) fabricated by subsequent additional imprinting at 90° on single patterned P3HT film. (C) Pristine P3HT film (0D), and (D) cross-sectional profiles of (A) and (B).

properties of the patterned EC devices. While P3HT is a representative hole transporting material and is frequently used for organic devices such as photovoltaics and transistors,[20,21] its application to electrochromic devices is relatively rare despite its unique electrochromic properties and the easy processability.[22]

RESULTS AND DISCUSSION

Patterning of P3HT in 1D and 2D by PDMS Imprinting. P3HT films were nanopatterned *via* soft lithography performed at room temperature. A PDMS mold consisting of periodic 170 nm width lines separated by 80 nm wide gaps was employed in the nanopatterning process (Figure S1, Supporting Information). Nanogratings (1D) were first patterned on a P3HT film by a single imprinting without any pressure. However, the depth of the gratings was rather small: 25 nm as determined from AFM. Under a pressure of 5 kg, the depth in the 1D patterning process was increased to 47 nm. Thus, 1D and 2D patterning was carried out under pressure. As verified by AFM measurements, 1D nanogratings of the PDMS in a 1 × 1 cm^2 area were successfully and homogeneously transferred to the entire area of the P3HT film. The width and gap between the lines were 362 and 110 nm, respectively (Figure 1). The nanogratings on the P3HT were wider in period and shallower in depth than those of the PDMS master.

Additional contact pressing in a 90° direction under the same pressure produced nanopillars (2D) on the single patterned P3HT. Nanopillar patterns (2D) were generated with dimensions of 380 nm in width, 60 nm in height, and a pillar separation of about 80 nm in the double-pressed area. As shown in Figure 2, the edge image clearly traced the first (1D) and second (but single-pressed) patterns, as well as the second pattern at the crossed (double-pressed) area. In the area pressed second with a single press, the height was slightly lower (~40 nm) than the area pressed first. This was possibly due to the evaporation of residual solvent. The height was increased in the cross (double) patterned area.

The average roughness (R_a) values in a 5 μm × 5 μm area were 1.1, 11.3, and 18.3 nm for the pristine (0D), 1D, and 2D patterned films, respectively. This indicates

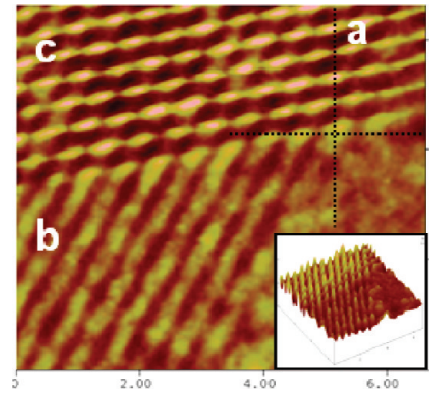

Figure 2. Edge AFM image of 2D patterned P3HT film that was first (a, 1D) and second (b, but single-pressed) patterned, and second patterned at the crossed (c, double-pressed) area (inset: 3D image).

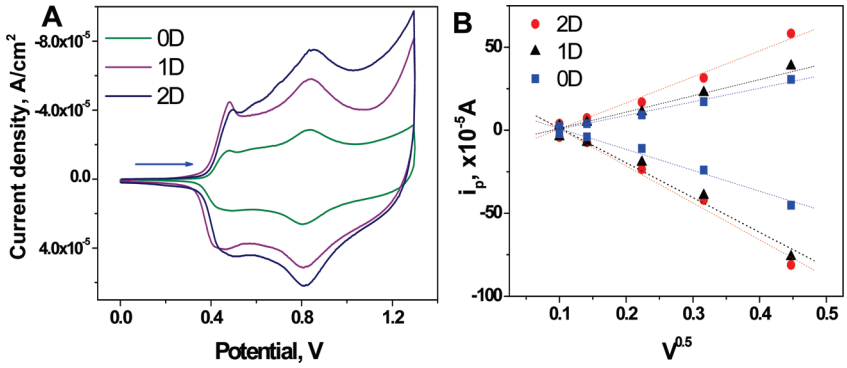

Figure 3. (A) Cyclic voltammogram of P3HT films at 10 mV/s. (B) Plot of cathodic and anodic peak current according to the square root of the scan rate ($v^{0.5}$).

that the roughness of the film increased as the dimension of the pattern increased. Such a scenario is possibly due to increased ordering in the P3HT domain. It has been reported that P3HT chain alignment can be enhanced during nanograting imprinting on a P3HT film. The chain alignment is induced by polymer flow to nanocavities, thus generating high degree (100) chain alignment.[23] After patterning, the surface area of the films increased to 25.2, 25.7, and 26.8 μm^2 for the pristine (0D), 1D, and 2D patterned films, respectively. The surface areas attained from the simulation using Matlab were in good agreement with the AFM results as 25.4 and 26.9 μm^2 for the 1D and 2D patterns, respectively, when the geometry of the column (1D) and pillars (2D) were assumed to be triangular and conical structure, respectively.

Electrochemical Properties of Nanopatterned P3HT. Cyclic voltammetry (CV) measurements for the pristine (0D), 1D, and 2D patterned P3HT films were performed in a three-electrode system using a solution of 0.1 M $LiClO_4$ in acetonitrile and a scan rate of 10 mV/s from 0 to 1.3 V (Figure 3A). All films exhibited several redox peaks centered at ~0.49 and 0.83 V (*vs* Ag/AgCl). A transition between the polaronic and bipolaronic states[22] was observed. This transition is detailed in the following expression:

$$\underset{\text{(neutral)}}{P3HT^0} + ClO_4^- \underset{\text{red}(+e^-)}{\overset{\text{Ox}(-e^-)}{\rightleftharpoons}} \underset{\text{(polaron, radical cation)}}{P3HT^{+\bullet}ClO_4^-} \underset{\text{red}(+e^-)}{\overset{\text{Ox}(-e^-)}{\rightleftharpoons}} \underset{\text{(bipolaron, dication)}}{P3HT^{2+}2ClO_4^-} \quad (1)$$

In eq 1, ClO_4^- is a counteranion and e^- denotes an electron. It should be noted that the redox peaks of the 1D and 2D patterned films were shifted with a much higher intensity than those of the unpatterned film (0D). It has been reported that P3HT films with a high degree of ordering or regioregularity exhibit larger peak currents with a peak shift.[22,24,25] Thus, P3HT chain alignment may be enhanced during nanoimprinting on a P3HT film, as nanoconfinement induces chain alignment in P3HT nanostructures and generates a high degree (100) of chain alignment.[23] The X-ray diffraction (XRD) results showed that the intensity decrease of the (100) peak at 5.2° was 24% (1D) and 61% (2D) (Figure S2A, Supporting Information). This result is in good agreement with results from the literature regarding changes in the out-of-plane detecting mode P3HT and may be attributed mainly to changes in P3HT chain ordering edge-on to the vertical ordering.[23] In addition, the (100) diffraction peak was shifted from 5.15° (0D) to 5.20° (1D) and 5.25° (2D), and the interlayer spacing determined from the Bragg equation was shifted from 17.15 to 16.98 and 16.82 Å for 0D, 1D, and 2D, respectively. The P3HT chain spacing became smaller after nanopatterning, thus it provided lower resistance to charge carriers to transport through the polymer chains.[22] The increase in absorbance at the shoulder band (>570 nm) in the nanoimprinted gratings (Figure S2B) is due to the increased $\pi-\pi^*$ stacking and interchain interactions between P3HT chains.[23,26] The $\pi-\pi^*$ chain alignment could be quantified by comparing absorbance ratios at ~590 nm with absorbance maxima (~530 nm) in different samples. The absorbance ratio was 0.49 for 0D and increased to 0.54 for 1D and 0.67 for 2D. This indicates that the $\pi-\pi^*$ interchain stacking was improved by nanopatterning, but the change was small (less than 30%).

The major contribution to the increased current arises from the extra shoulder peak (0.5−0.8 V) between the first and second redox processes. The shoulder peak is indicative of the formation of new polymer domains that may facilitate charge transport through the P3HT electrode. This redox process is reversible over repeated voltammetric scans with no electrochemical degradation during cycles between the polaronic and bipolaronic (neutral and oxidized) states. As the redox peaks consisted of two peaks plus shoulder peaks, all of the CV measurements were deconvoluted ($R^2 > 0.999$) based on Gaussian peaks (Figure S3, Supporting Information) to quantify the peak current and determine charge transport at the electrode nanopatterned in different dimensions.

In an electrochemical process that is linear-diffusion-driven, the peak current is related to the electrode area

and the square root of the scan rate ($\nu^{1/2}$) according to the Randles−Sevcik equation:[27]

$$i_p = (2.69 \times 10^5) n^{3/2} A C D_f^{1/2} \nu^{1/2} \quad (2)$$

In eq 2, i_p is the peak current, n is the number of electron transfer, D_f ($cm^2\ s^{-1}$) is the diffusion coefficient, A is the electrode area (cm^2), C is the solution concentration (mol cm^{-3}), and ν is the scan rate ($V\ s^{-1}$). By plotting the anodic and cathodic peak current obtained at ~0.57 and ~0.54 V against $\nu^{1/2}$ for both the pristine and nanostructured electrodes, linear relationships (shown in Figure 3B) were observed. Both the anodic and cathodic currents were linearly correlated to $\nu^{1/2}$, which indicates that electrochemical doping of the entire P3HT film occurred with no irreversible electrochemical reaction. Furthermore, the linear relationship of i_p against $\nu^{1/2}$ suggests that the behavior of the electrochemical processes at the P3HT electrode is mainly controlled by the diffusion of ClO_4^- counterions associated with the redox processes at the P3HT electrode. The D_f values for the patterned electrodes were determined from the slope in Figure 3B; they are summarized in Table 1. The D_f values for the oxidation of the electrodes are larger than those of the reduction process. In the electrochemical doping process of a polythiophene film, ClO_4^- ions penetrate into the polymer and promote movement in nearby polymer molecules, which favors penetration of further ClO_4^- into the polymer. Movement and ionic penetration proceed on the surface in a sigmoidal fashion, and thus, the charge transport is facilitated. Upon dedoping in the reduction step, the orientation of the P3HT chains switches from a "lying-down" configuration to an "on-edge" configuration with the alkyl chains being normal to the electrode surface.[28] Thus, in the reduction, it takes more time to remove the ions that have penetrated into the polymer layer into the electrolyte solution. The D_f values for reduction are therefore smaller than those for oxidation. Interestingly, the diffusion coefficient for the patterned electrode was much larger than that of the unpatterned electrode. Furthermore, D_f was larger as the dimension of the pattern was increased (Table 1). The D_f for the 2D patterned electrode was the largest among the P3HT electrodes. The diffusion coefficient for the oxidation process in 2D reached 6.67×10^{-9} cm^2/s, which is three times higher than that of the pristine film. The D_f value for the dedoping of ClO_4^- counterions for coloration (3.36×10^{-9} cm^2/s) was also higher in the 2D patterned electrode. The diffusion coefficients in this work are larger than the reported values for P3HT (10^{-10}~10^{-14} cm^2/s) films in contact with liquid electrolytes.[29,30] This is possibly due to the ordering of P3HT in this work through patterning. In addition, the D_f value of the 2D patterned P3HT is an order of magnitude higher than those of conducting polymer films based on PEDOT[31,32] for electrochromic devices. Therefore, as discussed in the literature,[33,34] the electronic response of a conductive polymer-based device may improve as charge transport through the nanostructured electrode is enhanced due to fast diffusion at the electrode. To prove such a concept, the nanostructured electrodes were incorporated into an electrochromic (EC) window and test for diffraction control.

TABLE 1. Diffusion Coefficients of P3HT Films

	diffusion coefficient (cm^2/s)		
	0D	1D	2D
oxidation	2.16×10^{-9}	5.99×10^{-9}	6.67×10^{-9}
reduction	1.05×10^{-9}	1.48×10^{-9}	3.36×10^{-9}

TABLE 2. Electrochromic Properties of ECDs with 0D, 1D, and 2D Patterning

		response time, s[a]			E_e, cm^2/C[b]	
potential step, V	sample	coloration	bleaching	Δabs	E_c	E_b
−1 to 2	0D	6.8	4.3	0.30	100	246
	1D	5.0	3.0	0.35	218	413
	2D	2.2	1.4	0.38	278	467
−2 to 2	0D	1.5	1.6	0.42	184	320
	1D	1.0	0.7	0.50	262	600
	2D	0.6	0.6	0.54	397	697
−2 to 2.5	2D	0.7	0.7	0.56	169	639
−2.5 to 2.5		0.7	0.6	0.43	139	589

[a]Response time for 70% of full switch. [b]Electrochromic efficiency (E_e), coloration (E_c), and bleaching efficiency (E_b).

Electrochromic (EC) Properties of Nanostructured P3HT Electrodes. Transmissive-type EC devices were prepared with P3HT films as a working electrode and ITO glass as a counter electrode. The liquid electrolyte solution described in Figure 3A was introduced between the two electrodes. The EC devices exhibited a reversible color change from red to transparent blue when −2 to 2 V was applied. The EC response required a larger potential step than was expected from the solution CV. This reflects the fact that the CV of the two-electrode system exhibited broad redox peaks at +2 and −2 V for oxidation and reduction, respectively, for the 2D patterned EC electrode (Figure S4, Supporting Information). As evident in Table 2, the color change was smaller when −1/2 or −2.5/2.5 V was applied to the EC devices. This indicates that the color change corresponds to redox reactions that consume charges generated at the peak potential in the two-electrode CV. The UV−vis absorbance changes of the EC cells from a neutral (−2 V) to an oxidized (2 V) state are shown in Figure 4. The red color in the neutral state changed to transparent blue and an absorption maximum at 537 nm decreased when the P3HT was oxidized at 1.2 V.

The optical responses of the P3HT films in a liquid electrolyte under step potentials of −1 to 2 V and −2 to 2 V, which correspond to the redox process for dedoping and p-type doping, respectively, are shown in

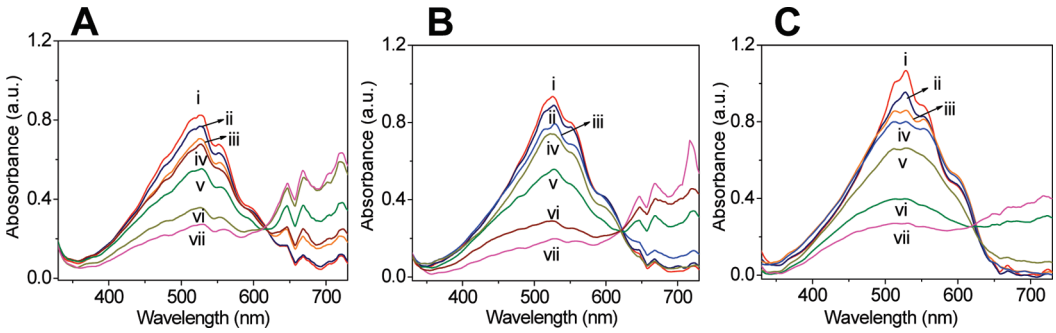

Figure 4. UV−vis absorbance spectra of pristine (A), 1D (B), and 2D (C) electrochromic devices (ECDs) from neutral to oxidized states at the applied potential; (i) −2 V, (ii) −1 V, (iii) 0 V, (iv) 0.9 V, (v) 1.2 V, (vi) 1.5 V, and (vii) 2.0 V.

Figure 5A.[28,35] High optical reversibility and coulommetric reversibility were observed with a switching time of 20 s. The optical contrast (Δabs) and coloratioamperometric plot of i_p against time under a step potential (Figure 5B) exhibited typical first-order differential decay. The i_p drops faster to reach saturation in the 1D and 2D patterned films, suggesting improvement in charge transport through nanopatterning. As a result, the response times for both coloration and bleaching were significantly reduced in the patterned P3HT. Furthermore, the electrochromic efficiency (E_e), including the coloration (E_c) and bleaching efficiency (E_b), was higher as the dimension of the pattern was increased. The E_e was maximized in the 2D patterned P3HT film (Table 2). These results could be attributed to facilitated charge transfer through the nanostructured EC electrode by increasing the dimension of the pattern. It is consistent with observations when the diffusion coefficient was determined (described above). The bleaching (p-doping) process was faster than the coloration process (dedoping), which matched the results on diffusion coefficients described above in Table 1. The E_e increased as the diffusion coefficient (D_f) from eq 2 and pattern dimension were increased. Surprisingly, the plots of E_e *versus* $D_f^{0.5}$ were linearly correlated over a wide range of E_e values determined at different potential steps for both coloration and bleaching, as shown in Figure 5C. The slope of the linear plot attained with a larger potential step of −2 V/2 V (filled circles) was higher than that plot derived with a low potential step of −1 V/2 V (open circles). Such a finding indicates that the dedoping state of the polymer was maximized at −2 V.

Switching times are dominated by the diffusion of counterions through the films during the redox step. Fast optical response times (in seconds) were observed in the patterned systems because the patterned morphology of the polymer promotes the mobility of charge compensating counterions. The response time for bleaching is faster when compared to that for coloration, which agrees well with the larger D_f associated with the bleaching in Table 1.

Reversible Electrochromic Diffraction from a Nanostructured EC Window. Since improved EC properties were observed using the patterned ECD, electrochromic diffraction control was explored to determine whether a light diffraction pattern could be generated by a patterned electrochromic device. The diffraction light intensity and, thus, the efficiency (DE)[36] of a grating depend on the optical properties (the absorptivity *k* and the refractive index *n*) of the grating material. Therefore, it is possible to use an electrochemical stimulus to modulate the DE of a redox-active grating. Light diffraction was examined by *in situ* detection of the diffracted light (I_d) from the cell under a 635 nm laser, by both transmittive and reflective mode. A schematic of the measurement (Figure 6A) and photographs of the diffracted light image from a patterned ECD at −2 V (colored) and +2 V (bleached) are shown in Figure 6. The 1D and 2D cells

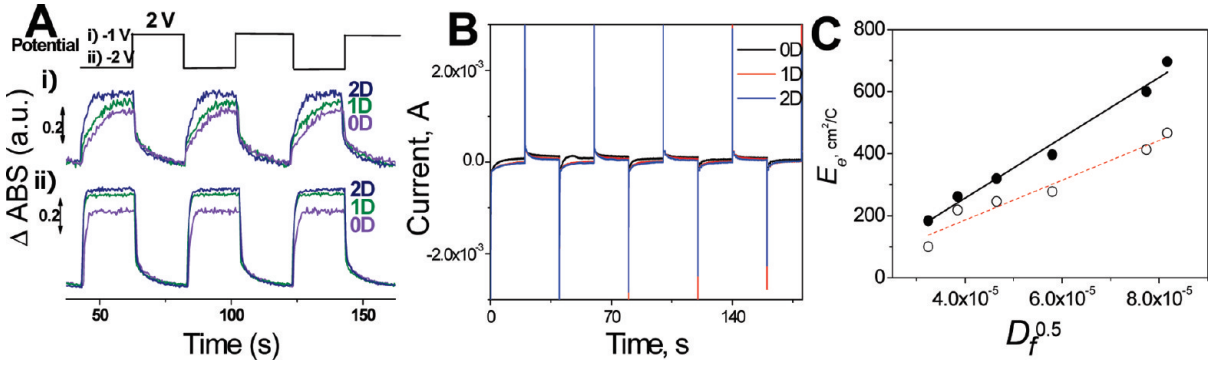

Figure 5. (A) Optical responses of 0D, 1D, and 2D ECDs containing liquid electrolytes for 20 s per step measured at 537 nm; (i) at −1 V and +2 V and (ii) at −2 V and +2 V. (B) Coloratioamperometric plot of i_p against time for 0D, 1D, and 2D ECDs at −1 and +2 V applications for 20 s per step. (C) Linear plot of electrochromic efficiency (E_e) for ECDs at −2 V/2 V (filled circle) and −1 V/2 V (open circle) against the square root of the diffusion coefficient ($D_f^{0.5}$).

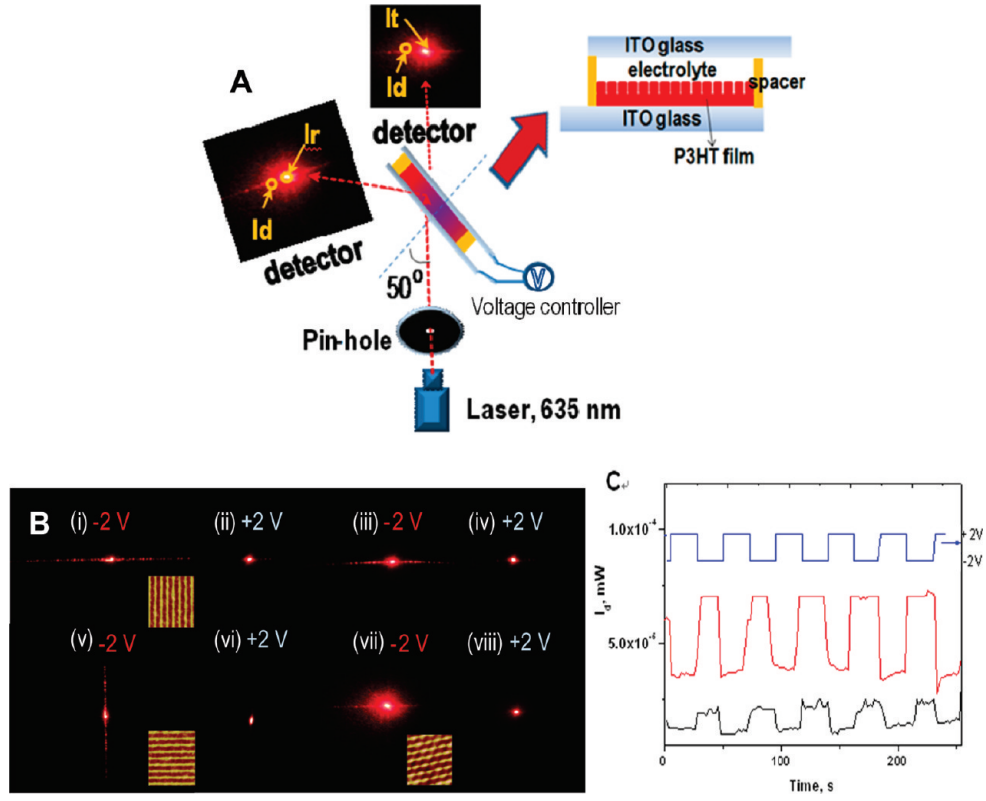

Figure 6. (A) Schematic of the patterned ECD and light diffraction measurement with a 635 nm laser diode. (B) Photographs of the diffracted light images from the patterned ECD; (i−iv) 1D ECD with vertical pattern (inset) showing reversible diffraction modulation at −2 V (colored) and +2 V (bleached); (v,vi) 1D ECD with horizontal pattern (inset) at −2 V (colored) and +2 V (bleached); (vii,viii) 2D patterned ECD at colored (−2 V) and bleached (+2 V) states, respectively. (C) Diffraction response of patterned ECDs on a step potential of +2/−2 V (blue line) in transmitted mode (red line) and reflected mode (black line) for a 2D cell.

showed fast and reversible light modulation within a second, as shown in Figure 6B. In the 1D patterned cell, the diffracted light was observed to be perpendicular to the patterned direction (Figure 6B, i and v), as the 1D grating patterns only allow light passage through the direction perpendicular to the grating direction. The intensity of the diffracted light was weak, and DE was determined as 1 and 9% for transmitted I_d (DE_t) and reflected I_d (DE_r), respectively, when the cell was at +2 V (bleached state). The diffracted light returned to its original intensity when −2 V was applied to the cell obtaining 2 and 12% for DE_t and DE_r, respectively, and was switchable between the potential step of +2/−2 V, as shown in Figure 6B. The light diffraction from the 2D patterned ECD was omnidirectional and much stronger when compared to the 1D patterned cell (Figure 6B, vii)). The DE_t and DE_r in 2D decreased from 5 and 13% to 2 and 8% when the cell was switched from −2 to +2 V. The switching efficiency (R_{DE}), as determined from the ratio between the DE_t in the colored and bleached states, was 2 and 2.5 for the 1D and 2D patterned cells, respectively. This result indicates that EC control of the diffraction light intensity could be more effective in the 2D patterned cell due to its improved EC properties. Moreover, the diffraction intensity was reversibly controlled by the alternative step potential of +2/−2 V, either in transmission or reflection mode, in the 2D patterned cell, as shown in Figure 6C.

A more thorough account of EC diffraction is forthcoming, including impedance analysis on nanopatterned P3HT and polarization effects on electrochromism. However, a key aspect of note is that the overall redox behavior of the patterned P3HT electrode could be applied to an electrically driven diffraction lighter, where ion diffusion is accompanied by a redox process control. This would allow for control over both color change and the refractive index.

In summary, the charge transport characteristics of P3HT films with one-dimensional grating and two-dimensional crossed line patterns facilitated charge transport with an increased diffusion coefficient (D_f) for counteranions. This resulted in an improved response time and higher coloration and bleaching efficiencies for P3HT-based electrochromic devices. In patterned cells, diffraction modulation was achieved *via* an electrochromic operation. The switching efficiencies (R_{DE}) of the 1D and 2D patterned cells were 2 and 2.5, respectively, indicating that EC control of diffraction light intensity may be more effective in the 2D patterned cell due to its improved EC properties. Moreover, diffraction intensity was reversibly controlled by an alternative step potential of +2/−2 V

in the 2D patterned cell either in transmittive or reflected mode. Future patterning studies of thin films fabricated from P3HT or its derivatives will contribute to an improved understanding of charge transport in nanostructured conductive polymers and foster the development of advanced EC devices with improved optical, ionic, and electronic transport properties.

METHODS

Poly(3-hexylthiophene) (P3HT, $M_w = 25\,000$ g · mol^{-1}) was purchased from Rieke Metals Inc. 1,2-Dichlorobenzene was obtained from Sigma-Aldrich. PDMS and a curing agent (Sylgard 184) were purchased from the Dow Corning Corporation. Lithium perchlorate and acetonitrile were obtained from Sigma-Aldrich.

A 2 wt % P3HT solution in 1,2-dichlorobenzene was spin-coated at 700 rpm for 40 s on an ITO glass electrode (13 Ω/square). A P3HT nanopatterned film was then generated *via* soft lithography,[18] a simple contact-pressing method that employs a nanopattern replicated PDMS mold. A nanopatterned photoresist template on a silicon wafer was provided by Keumho Petrochemicals and used for the replication (Figure S1, Supporting Information). The template consisted of nanogratings in a 1 cm × 1 cm area with a width of 250 nm and a height of 90 nm. The gap between the gratings was 15 nm. A detailed PDMS mold fabrication method is described elsewhere.[37] A replicated PDMS nanograting mold (1.3 g in weight) consisting of periodic 170 nm width lines separated by 80 nm wide gaps was introduced for the nanoimprinting. The trenches of the gratings were 80 nm in depth. Nanoimprinting was carried out at room temperature. P3HT nanogratings (1D) were obtained through a single imprinting. After full contact between the P3HT film and the PDMS patterned area was established, pressing was performed for 3 min with PDMS mold at a pressure of 5 kg. This resulted in a wet surface flow-induced pattern. Additional contact pressing in a 90° direction was carried out under pressure of 5 kg for 5 min at room temperature to produce nanopillars (2D) on the surface of single patterned P3HT. The pristine and patterned films were both annealed under vacuum at 100 °C for 10 min to evaporate residual solvent in the film.

A conventional three-electrode system consisting of the P3HT-coated ITO glass as the working electrode and Ag/AgCl and Pt wire as the counter electrode was used for cyclic voltammetry measurements. Lithium perchlorate ($LiClO_4$, 0.1 M) in acetonitrile was employed as a supporting electrolyte. An electrochromic device with two electrodes was fabricated using P3HT-coated ITO glass as the working electrode and bare ITO glass as the counter electrode. A liquid electrolyte containing 0.1 M $LiClO_4$ in acetonitrile was isolated between the two electrodes by a spacer.

The conductivities of the 0D, 1D, and 2D patterned P3HT films were examined using a top-contact four-point probe. Conductivity was determined to be 0.10, 0.11, and 0.13 S/cm for 0D, 1D, and 2D samples, values that are comparable to previously reported values.[38] The pattern-induced conductivity increment was 30% (30 mS/cm). This small change in conductivity caused by patterning may be attributed to the unpatterned P3HT part of the film. As shown in Figure 1D, the maximum height of the gratings is 60 nm, while the thickness of the P3HT film was 100 nm. Thus, the thickness of the unpatterned P3HT is ~40 nm, which connects the P3HT conductive channel to yield small conductivity change.

Electrochromic properties were determined by an *in situ* spectro-electrochemical setup.[8−12] The coloration efficiency and response time of the ECDs were determined at the absorption max under a square-wave switching potential using a chronocoulometry in liquid electrolyte having an EC window size of 1.0 × 1.0 cm^2. The EC response time for coloration and bleaching was determined at a 70% absorption change[11,12] under the given step potentials. The electrochromic efficiency (E_e) including the coloration and bleaching efficiency was determined by dividing the Δabs by the injected/ejected charge per unit area.[39]

A 635 nm diode laser with an intensity of 2.1 mW was used to measure the diffraction from the patterned electrochromic devices at colored and bleached states (Figure 6A). The intensities of the reflected (I_r), transmitted (I_t), and I_a ("$I_d + I_r$" or "$I_d + I_t$") light were determined using a photodetector. I_d was calculated as the difference between the I_a and I_t or I_r. UV−vis spectra were attained with an Avaspec-2048 fiber optic spectrometer. The nanopattern transfer from the PDMS stamp to the composite films was carried out using Nanoimprint (HIS-400U, Hutem Inc.). The thickness of the polymer films was determined *via* profilometry measurements performed with an Alpha Step profilometer (Tencor Instruments, Alpha-Step IQ). The accuracy of the profilometer was 1 nm. Atomic force microscopy (AFM) was carried out in tapping mode at room temperature with a Dimension 3100 SPM equipped with a Nanoscope IVa (Digital Instruments, Santa Barbara, CA).

Acknowledgment. This work was supported by the National Research Foundation (NRF) grant funded by the Korea government (MEST) through the Active Polymer Center for Pattern Integration (No. R11-2007-050-00000-0) and Ministry of Knowledge Economy (MKE), New & Renewable Energy Technology Development Program.

Supporting Information Available: Atomic force microscope (AFM) images are available for the nanopattern master; XRD graphs and UV−vis spectra of pristine (0D), 1D, and 2D patterned P3HT film; analyses of redox peaks based on Gaussian multipeak deconvolution of cyclic voltammograms of 0D, 1D, and 2D patterned P3HT films using Origin 7.5; and cyclic voltammogram of two-electrode P3HT-based ECD scanning between −2 to 2 V at 0.1 V/s. This material is available free of charge *via* the Internet at http://pubs.acs.org.

REFERENCES AND NOTES

1. Yu, G.; Gao, J.; Hummelen, J. C.; Wudl, F.; Heeger, A. J. Polymer Photovoltaic Cells: Enhanced Efficiencies *via* a Network of Internal Donor−Acceptor Heterojunctions. *Science* **1995**, *270*, 1789–1791.
2. Kim, Y.; Do, J.; Kim, J.; Yang, S. Y.; Malliaras, G. G.; Ober, C. K.; Kim, E. A Glucose Sensor Based on an Organic Electrochemical Transistor Structure Using a Vapor Polymerized Poly(3,4-ethylenedioxythiophene) Layer. *Jpn. J. Appl. Phys.* **2010**, *49*, 01AE10-1–01AE10-10.
3. Kim, Y.; Yun, C.; Jadhav, P.; You, J.; Kim, E. Emissive Pattern Formation by the Photoreaction of Poly(*p*-phenylene vinylene). *Curr. Appl. Phys.* **2009**, *9*, 1088–1092.
4. Kim, D. C.; Lee, T. W.; Lee, J. E.; Kim, K. H.; Cho, M. J.; Choi, D. H.; Han, Y. D.; Cho, M. Y.; Joo, J. S. New Semiconducting Multi-branched Conjugated Molecules Bearing 3,4-Ethylenedioxythiophene-Based Thiophenyl Moieties for Organic Field Effect Transistor. *Macromol. Res.* **2009**, *17*, 491–498.
5. Kim, J.; Kim, Y.; Kim, E. Electrochromic Pattern Formation by Photo Cross-Linking Reaction of PEDOT Side Chains. *Macromol. Res.* **2009**, *17*, 791–796.
6. Dobrokhotov, V. V.; McIlroy, D. N.; Norton, M. G.; Berven, C. A. Transport Properties of Hybrid Nanoparticle—Nanowire Systems and Their Application to Gas Sensing. *Nanotechnology* **2006**, *16*, 4135–4142.
7. Ziebarth, J. M.; Saafir, A. K.; Fan, S.; McGehee, M. D. Extracting Light from Polymer Light-Emitting Diodes Using Stamped Bragg Gratings. *Adv. Funct. Mater.* **2004**, *14*, 451–456.
8. Baek, J.; Kim, Y.; Kim, E. Growth and Electrochromic Properties of PEDOT Layer on TiO_2 Nanoparticles. *J. Nanosci. Nanotechnol.* **2008**, *8*, 4851–4855.

9. Kim, Y.; Kim, E. Complementary Electrochromic Windows with Conductive Nanocomposite Thin Films. *Curr. Appl. Phys.* **2008**, *8*, 752–754.
10. Kim, Y.; Baek, J.; Kim, M.-H.; Choi, H.-J.; Kim, E. Electrochromic Nanostructures Grown on a Silicon Nanowire Template. *Ultramicroscopy* **2008**, *108*, 1224–1227.
11. Kim, Y.; Kim, E. Electrochromic Properties of Nanochromic Windows Assembled by the Layer-by-Layer Self-Assembly Technique. *Curr. Appl. Phys.* **2006**, *6*, e202–e205.
12. Kim, Y.; Yang, S. Y.; Kim, E. Electrochromic Properties of Asymmetric 4,4′-Bipyridinium Nanocomposites with Inorganic Nanoparticles. *J. Nanosci. Nanotechnol.* **2010**, *10*, 263–268.
13. Kim, E.; Jung, S. Layer-by-Layer Assembled Electrochromic Films for All-Solid-State Electrochromic Devices. *Chem. Mater.* **2005**, *17*, 6381–6387.
14. Cho, S. I.; Kwon, W. J.; Choi, S.-J.; Kim, P.; Park, S.-A.; Kim, J.; Son, S. J.; Xiao, R.; Kim, S.-H.; Lee, S. B. Nanotube-Based Ultrafast Electrochromic Display. *Adv. Mater.* **2005**, *17*, 171–175.
15. Brezesinski, T.; Rohlfing, D. F.; Sallard, S.; Antonietti, M.; Smarsly, B. M. Highly Crystalline WO_3 Thin Films with Ordered 3D Mesoporosity and Improved Electrochromic Performance. *Small* **2006**, *2*, 1203–1211.
16. Zhang, F.; Nyberg, T.; Inganäs, O. Conducting Polymer Nanowires and Nanodots Made with Soft Lithography. *Nano Lett.* **2002**, *2*, 1373–1377.
17. Beh, W. S.; Kim, I. T.; Qin, D.; Xia, Y.; Whitesides, G. M. Formation of Patterned Microstructures of Conducting Polymers by Soft Lithography, and Applications in Microelectronic Device Fabrication. *Adv. Mater.* **1999**, *11*, 1038–1041.
18. Admassieaz, S.; Inganäs, O. Electrochromism in Diffractive Conducting Polymer Gratings. *J. Electrochem. Soc.* **2004**, *151*, H153–H157.
19. Choi, J.; Kumar, A.; Sotzing, G. A. Nanopatterned Electrochromic Conjugated Poly(terthiophene)s *via* Thermal Nanoimprint Lithography of Precursor Polymer. *J. Macromol. Sci. A* **2007**, *44*, 1305–1309.
20. Jeffries-El, M.; McCullough, R. D. Conjugated Polymers: Theory, Synthesis, and Characterizations. In *Handbook of Conducting Polymers*; Skotheim, T. A., Reynolds, J. R., Eds.; CRC Press: Boca Raton, FL, 2007; pp 9-1−9-2.
21. Sirringhaus, H.; Brown, P. J.; Friend, R. H.; Nielsen, M. M.; Bechgaard, K.; Langeveld-Voss, B. M. W.; Spiering, A. J. H.; Janssen, R. A. J.; Meijer, E. W.; Herwig, P.; *et al.* Two-Dimensional Charge Transport in Self-Organized, High-Mobility Conjugated Polymers. *Nature* **1999**, *401*, 685–688.
22. Huang, J.-H.; Yang, C.-Y.; Hsu, C.-Y.; Chen, C.-L.; Lin, L.-Y.; Wang, R.-R.; Ho, K.-C.; Chu, C.-W. Solvent-Annealing-Induced Self-Organization of Poly(3-hexylthiophene), a High-Performance Electrochromic Material. *ACS Appl. Mater. Interfaces* **2009**, *1*, 2821–2828.
23. Aryal, M.; Trivedi, K.; Hu, W. Nano-confinement Induced Chain Alignment in Ordered P3HT Nanostructures Defined by Nanoimprint Lithography. *ACS Nano* **2009**, *3*, 3085–3090.
24. Ratcliff, E. L.; Jenkins, J. L.; Nebesny, K.; Armstrong, N. R. Electrodeposited, "Textured" Poly(3-hexyl-thiophene) (e-P3HT) Films for Photovoltaic Applications. *Chem. Mater.* **2008**, *20*, 5796–5806.
25. Skompska, M.; Szkurlat, A. The Influence of the Structural Defects and Microscopic Aggregation of Poly(3-alkylthiophenes) on Electrochemical and Optical Properties of the Polymer Films: Discussion of an Origin of Redox Peaks in the Cyclic Voltammograms. *Electrochim. Acta* **2001**, *46*, 4007–4015.
26. Chen, T.-A; Wu, X.; Rieke, R. D. Regiocontrolled Synthesis of Poly(3-alkylthiophenes) Mediated by Rieke Zinc: Their Characterization and Solid-State Properties. *J. Am. Chem. Soc.* **1995**, *117*, 233–244.
27. Bard, A. J.; Faulkner, L. R. *Electrochemical Methods: Fundamentals and Applications*, 2nd ed.; Wiley: New York, 2001; pp 228−243.
28. Schopf, G.; KoBmehl, G. Polythiophenes—Electrically Conductive Polymers. *Advances in Polymer Science*; Springer: Berlin, 1997; pp 51−80.
29. Mills, T.; Kaake, L. G.; Zhu, X.-Y. Polaron and Ion Diffusion in a Poly(3-hexylthiophene) Thin-Film Transistor Gated with Polymer Electrolyte Dielectric. *Appl. Phys. A: Mater. Sci. Process.* **2009**, *95*, 291–296.
30. Kaneto, K.; Agawa, H.; Yoshino, K. Cycle Life, Stability, and Characteristics of Color Switching Cells Utilizing Polythiophene Films. *J. Appl. Phys.* **1987**, *61*, 1197–1205.
31. Lock, J. P.; Lutkenhaus, J. L.; Zacharia, N. S.; Im, S. G.; Hammond, P. T.; Gleason, K. K. Electrochemical Investigation of PEDOT Films Deposited *via* CVD for Electrochromic Applications. *Synth. Met.* **2007**, *157*, 894–898.
32. Sonmez, G.; Schottland, P.; Reynolds, J. R. PEDOT/PAMPS: An Electrically Conductive Polymer Composite with Electrochromic and Cation Exchange Properties. *Synth. Met.* **2005**, *155*, 130–137.
33. Tchepournaya, I.; Vasilieva, S.; Logvinov, S.; Timonov, A.; Amadelli, R.; Bartak, D. Electrochemical Synthesis and Characterization of Redox Polymer Nanostructures. *Langmuir* **2003**, *19*, 9005–9012.
34. Anandan, V.; Rao, Y. L.; Zhang, G. Nanopillar Array Structures for Enhancing Biosensing Performance. *Int. J. Nanomed.* **2006**, *1*, 73–79.
35. Bélanger, M. Polythiophenes as Active Electrode Materials for Electrochemical Capacitors. In *Handbook of Thiophene-Based Materials*; Perepichka, I. F., Perepichka, D. F., Eds.; Wiley: West Sussex, UK, 2009; pp 579−580.
36. Schanze, K. S.; Bergstedt, T. S.; Hauser, B. T.; Cavalaheiro, C. S. P. Photolithographically-Patterned Electroactive Films and Electrochemically Modulated Diffraction Gratings. *Langmuir* **2000**, *16*, 795–810.
37. Chang-Yen, D. A.; Eich, R. K.; Gale, B. K. A Monolithic PDMS Waveguide System Fabricated Using Soft-Lithography Techniques. *J. Lightwave Technol.* **2005**, *23*, 2088–2093.
38. Osawa, S.; Ito, M.; Iwase, S.; Yajima, H.; Endo, R.; Tanaka, K. Effects of Molecular Weight on the Electrical Properties of Electrochemically Synthesized Poly(3-hexylthiophene). *Polymer* **1992**, *33*, 914–919.
39. Beaujuge, P. M.; Reynolds, J. R. Color Control in π-Conjugated Organic Polymers for Use in Electrochromic Devices. *Chem. Rev.* **2010**, *110*, 268–320.